2898 *Chem. Mater.* **2010,** *22,* 2898–2907
DOI:10.1021/cm100208a

CHEMISTRY OF MATERIALS
Article

Topotactic Nitrogen Transfer: Structural Transformation in Cobalt Molybdenum Nitrides

Stuart M. Hunter,[†] David Mckay,[†] Ronald I. Smith,[‡] Justin S. J. Hargreaves,*[,†] and Duncan H. Gregory*[,†]

[†]*WestCHEM, Department of Chemistry, University of Glasgow, Glasgow, G12 8QQ, United Kingdom, and* [‡]*ISIS Facility, Rutherford Appleton Laboratory, Chilton, Didcot, OX11 0QX, United Kingdom*

Received January 22, 2010. Revised Manuscript Received March 3, 2010

The temperature-programmed reaction of Co_3Mo_3N under H_2/Ar results in a new nitride with composition Co_6Mo_6N. Powder neutron diffraction (PND) studies have confirmed unequivocally that the compound possesses the η-12 carbide structure, in which N atoms are exclusively located at 8a crystallographic sites, as opposed to the 16c sites exclusively occupied in the Co_3Mo_3N phase. On this basis, it possible to rationalize the observation that 50% nitrogen loss occurs under the high-temperature reduction conditions employed. Reaction of the reduced η-12 phase under N_2/H_2 results in the regeneration of the η-6 Co_3Mo_3N nitride and return of nitrogen to the 16c sites (only). Although established for corresponding ternary carbide structures, the η-12 carbide structure is unprecedented in nitrides and a topotactic cycling between η-carbide structures is hitherto unknown. The ammonia synthesis activity of the η-6 nitride at ambient pressure and 400 °C is 167 μmol g^{-1} h^{-1}, whereas the η-12 structure is unstable and reverts back to the η-6 structure under reaction conditions. Studies of the magnetic properties of the cobalt molybdenum nitrides demonstrate that both the η-6 and η-12 nitrides exhibit no long-range magnetic ordering and are superparamagnetic, although the coercive field (H_c) observed in magnetization measurements is diminished in the reduced nitride.

Introduction

Transition-metal nitrides have been attracting interest, in terms of their mechanical, electronic, optical, magnetic, sustainable energy, and catalytic properties.[1−5] In terms of magnetism, some of the most interesting materials are ternary nitrides with the η-carbide or filled β-manganese structures where long-range magnetic order can be switched on with an appropriate choice of transition metals and valence electron counts.[6−8] In terms of catalysis, there has been resurgent interest since Volpe and Boudart[9] demonstrated that ammonolysis of oxide precursors can lead to the generation of high-surface-area nitrides, provided that high space velocities of ammonia and carefully selected ramp rates are applied.

Recently, the η-carbide structured (η-6) ternary molybdenum nitride, Co_3Mo_3N (abbreviated hereafter as 331), has attracted attention, as a result of its high efficacy in ammonia synthesis, particularly when doped with low levels of cesium.[10−18] Of particular interest to us is the tantalizing prospect that Co_3Mo_3N could also find application as a nitride catalyst for nitrogen transfer processes. We have designed several experiments to test precisely this premise.[19,20] In particular, in a series of temperature-programmed reactions, we have demonstrated that approximately 50% of the lattice nitrogen can be removed from the 331 phase. Such a reduction would therefore result in a Co:Mo:N ratio of 3:3:0.5 (or 6:6:1). Furthermore, it is possible to replenish this lost nitrogen in a reverse nitrogenation process. Evidence suggests that, given that the nitrogen content is reproducibly decreased (and increased) by 50% and that each reduction (oxidation) is accompanied by a constant

*Authors to whom correspondence should be addressed. E-mail addresses: justinh@chem.gla.ac.uk (J.S.J.H.), d.gregory@chem.gla.ac.uk (D.H.G.).

(1) *Chemistry of Transition Metal Carbides and Nitrides*; Oyama, S. T., Ed.; Blackie Academic and Professional: Glasgow, U.K., 1996.
(2) (a) Gregory, D. H. *J. Chem. Soc., Dalton Trans.* **1999**, 259. (b) Barker, M. G.; Blake, A. J.; Edwards, P. P.; Gregory, D. H.; Hamor, T. A.; Siddons, D. J.; Smith, S. E. *Chem. Commun.* **1999**, 1187. (c) Gregory, D. H.; O'Meara, P. M.; Gordon, A. G.; Siddons, D. J.; Blake, A. J.; Barker, M. G.; Hamor, T. A.; Edwards, P. P. *J. Alloys Compd.* **2001**, *317*, 237. (d) Gregory, D. H. *J. Mater. Chem.* **2008**, *18*, 2321. (e) Gregory, D. H. *Chem. Rec.* **2008**, *8*, 229.
(3) Furimsky, E. *Appl. Catal., A* **2003**, *240*, 1.
(4) Hargreaves, J. S. J.; Mckay, D. *Catalysis* **2006**, *20*, 84.
(5) Nagai, M. *Appl. Catal., A* **2007**, *322*, 178.
(6) Prior, T. J.; Battle, P. D. *J. Solid State Chem.* **2003**, *172*, 138.
(7) Prior, T. J.; Battle, P. D. *J. Mater. Chem.* **2004**, *14*, 3001.
(8) Prior, T. J.; Oldham, S. E.; Couper, V. J.; Battle, P. D. *Chem. Mater.* **2005**, *17*, 1867.
(9) Volpe, L.; Boudart, M. *J. Phys. Chem.* **1986**, *90*, 4874.
(10) Kojima, R.; Aika, K.-I. *Chem. Lett.* **2000**, 514.
(11) Kojima, R.; Aika, K.-I. *Appl. Catal., A* **2001**, *215*, 149.
(12) Kojima, R.; Aika, K.-I. *Appl. Catal., A* **2001**, *218*, 121.
(13) Kojima, R.; Aika, K.-I. *Appl. Catal., A* **2001**, *219*, 157.
(14) Jacbosen, C. J. H.; Brorson, M.; Sehested, T.; Teunissen, H.; Törnqvist, E. (Haldor Topsøe A/S). U.S. Patent 6,235,676, **1999**.
(15) Jacobsen, C. J. H. *Chem. Commun.* **2000**, 1057.
(16) Jacobsen, C. J. H.; Dahl, S.; Clausen, B. S.; Bahn, S.; Logadottir, A.; Norskov, J. K. *J. Am. Chem. Soc.* **2001**, *123*, 8405.
(17) Boisen, A.; Dahl, S.; Jacobsen, C. J. H. *J. Catal.* **2002**, *208*, 180.
(18) Mckay, D.; Hargreaves, J. S. J.; Rico, J. L.; Rivera, J. L.; Sun, X.-L. *J. Solid State Chem.* **2008**, *181*, 325.
(19) Mckay, D.; Gregory, D. H.; Hargreaves, J. S. J.; Hunter, S. M.; Sun, X. L. *Chem. Commun.* **2007**, 3051.
(20) Hargreaves, J. S. J.; Mckay, D. *J. Mol. Catal. A* **2009**, *305*, 125.

Published on Web 03/22/2010

change in cell volume for the η-carbide structure; the denitrogenation−nitrogenation process then is likely to be cycling between two line phases in the Co−Mo−N system.[19] In the equivalent Co−Mo−C system, two compounds are known to exist: Co_3Mo_3C (η-6) and Co_6Mo_6C (η-12).[21] (The Co_6Mo_6C phase is abbreviated as 661 hereafter.) There is no known analogous η-12 nitride.

In this paper, we report our initial studies of the nitrogenation and denitrogenation reactivity of the 331 phase and follow the changes in structure and stoichiometry via powder X-ray diffraction (PXD) and elemental analysis. However, it is only by using the scattering contrast from powder neutron diffraction (PND) that we have been able to understand fully these structural changes and trace the migration of nitrogen over the course of these processes (the electron density of N only accounts for ca. 3% of the total scattering by PXD). We have thus been able to locate nitrogen unequivocally within the lattice and understand the structural transformations in the Co−Mo−N system. As part of this same study, we have investigated how the magnetic properties of these η-carbide-type nitrides vary with structure and nitrogen stoichiometry.

Experimental Methods

Synthesis. The precursor to Co_3Mo_3N was prepared by adding 5.59 g of cobalt nitrate ($Co(NO_3)_2 \cdot 6H_2O$, Sigma−Aldrich, ≥98%) and 4.00 g of ammonium heptamolybdate ($(NH_4)_6Mo_7O_{24} \cdot 4H_2O$, Sigma−Aldrich, 81−83% as MoO_3) dissolved in 200 mL of distilled water. The resultant solution was heated to ~353 K. A purple precipitate, $CoMoO_4 \cdot nH_2O$ (confirmed by PXD;[22] see below) was obtained after vacuum filtration, and the precipitate was washed twice with distilled water and once with ethanol and then dried overnight at 423 K. The powder was then calcined at 773 K for 3 h in air. 1.00 g of the molybdate precursor was subsequently loaded into a vertical sintered quartz reactor (10.5 mm internal diameter) and heated under a 95 mL/min flow of ammonia (NH_3, BOC gases, grade N3.8). The furnace was programmed to heat the material in three stages; (i) from ambient temperature to 630 K at a rate of 5.6 K/min, (ii) to 720 K at a rate of 0.5 K/min, (iii) to 1058 K at a rate of 2.1 K/min. The furnace was held at this final temperature for 5 h. The sample was subsequently cooled to ambient temperature in the ammonia flow prior to passivation for 3 h, using a 100 mL/min flow of a 0.1% oxygen-containing gas mixture (95% N_2/4.9% Ar/0.1% O_2). PXD patterns indicated that the Co_3Mo_3N (331) phase was formed following further nitridation of the sample (0.4 g), using a 3:1 H_2/N_2 gas mixture (BOC, H_2 purity = 99.998%, N_2 purity = 99.995%) (60 mL/min, 2 h) (see Figure 1a). As discussed below, this nitriding step is essential to improve the crystallinity of the product. As described elsewhere,[19] the reduced Co_6Mo_6N (661) phase is prepared by the temperature-programmed denitridation of Co_3Mo_3N samples prepared in this manner, using a 3:1 H_2/Ar gas mixture (BOC, H_2 purity = 99.998%; Ar purity = 99.99%, 60 mL/min; 673 K, 4 h; 773 K, 1 h; 873 K, 1.5 h; 973 K, 0.5 h) (see Figure 1b). Regeneration of the 331 phase was performed using a 3:1 H_2/N_2 gas mixture at 973 K for 4 h.[19]

Characterization. *Diffraction Measurements.* PXD patterns were acquired with a Siemens Model D5000 powder diffractometer using Cu Kα radiation in Bragg−Brentano geometry. Scan times of 1 h over the range of 5°−85° 2θ were used for indexing, and scan times of 12 h were used over the range of 5°−105° 2θ for Rietveld refinement. All scans were performed with a step size of 0.02° 2θ. Time-of-flight (ToF) PND data were collected using the high-intensity Polaris diffractometer at the ISIS spallation source (Rutherford Appleton Laboratory). Powder samples (ca. 1 g) were contained in an 8-mm-diameter, thin-walled, cylindrical vanadium sample can. Diffraction data were collected using the two fixed ^{3}He tube detector banks at $\langle 2\theta \rangle$ = 35° and $\langle 2\theta \rangle$ = 145° and the fixed ZnS scintillation detector bank at $\langle 2\theta \rangle$ = 90°. Data were collected at 298 and 4.2 K. For subambient measurements, cans were loaded into a helium cryostat (AS Scientific Instruments, Abingdon, U.K.). The temperature of the samples was monitored using a RhFe sensor attached to the outside wall of the vanadium sample cans.

Rietveld refinements against both PXD and PND data were performed (separately) using the General Structure Analysis System (GSAS) through the EXPGUI interface.[23,24] The starting model for the PXD refinements used the previously published structure of Co_3Mo_3N[25] in cubic space group $Fd\bar{3}m$ for the standard samples prior to reaction under 25% Ar/H_2, and for post-reaction samples, several initial structural models were considered: (i) a η-6 structure modified to have a reduced nitrogen (50%) occupation of the 16*c* site, (ii) a structure isotypic with η-12 Co_6Mo_6C,[21] with N replacing C on the 8a position (at full occupancy), (iii) an η-carbide structure, in which N is statistically distributed across both the 8a and 16c sites. For each model (i−iii), initial cell parameters were obtained from indexing/least-squares cell refinement procedures, using Dicvol 04.[26] These same models were subsequently used for PND refinements. For the PND refinements, diffraction data from all three detector banks were used simultaneously in the final least-squares cycles in each case. Peak shapes in the PXD and PND diffraction profiles were modeled using the Type 2 profile function (a multiterm integration of the pseudo-Voigt function) and Type 3 profile function (a convolution of

(21) Newsam, J. M.; Jacobson, A. J.; McCandlish, L. E.; Polizzotti, R. S. *J. Solid State Chem.* **1988**, *75*, 296.
(22) Eda, K.; Uno, Y.; Nagai, N.; Sotani, N.; Whittingham, M. S. *J. Solid State Chem.* **2005**, *178*, 2791.
(23) Larson, A. C.; von Dreele, R. B. The General Structure Analysis System (GSAS), Report LAUR 086-748, Los Alamos National Laboratories, Los Alamos, NM, **2000**.
(24) Toby, B. H. *J. Appl. Crystallogr.* **2001**, *34*, 210.
(25) Jackson, S. K.; Layland, R. C.; zur Loye, H.-C. *J. Alloys Compd.* **1999**, *291*, 94.
(26) Boultif, A.; Louer, D. *J. Appl. Crystallogr.* **2004**, *37*, 724.

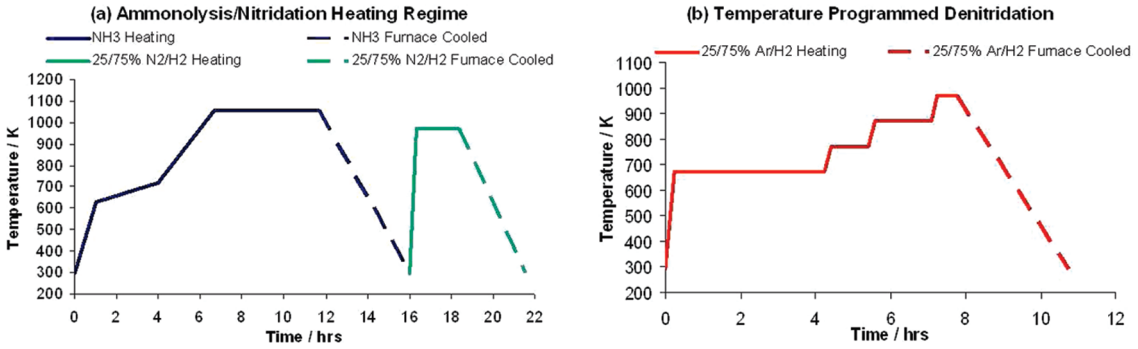

Figure 1. Heating regimes used in the preparation of (a) Co_3Mo_3N from $CoMoO_4 \cdot nH_2O$ and (b) Co_6Mo_6N from Co_3Mo_3N. (The dashed lines represent furnace cooling rather than a temperature-controlled, linear cooling rate.)

back-to-back exponentials with a pseudo-Voigt function) in GSAS respectively. The background was modeled using a reciprocal interpolation function (background function 8 in GSAS; PXD) and an exponential expansion function (background function 6 in GSAS; PND). The latter accounts for contributions at both low and high Q in ToF data. Structure refinements were started by fitting the background coefficients, scale factor, lattice parameters, and peak shapes and subsequently introduced atomic parameters and absorption factors (PND). After the refinements had stabilized, thermal coefficients were varied anisotropically. A very small amount of molybdenum metal was observed as an impurity phase in the Co_3Mo_3N samples. Attempts to refine the phase (with an approximate phase fraction of 1.5 wt %) and achieve convergence with reduced residuals were not satisfactory. Molybdenum reflections were excluded where possible (where overlap with the main phase was not significant). The vanadium sample can and the vacuum windows in the cryostat yielded a group of reflections that were excluded from the refinements. These excluded regions did not contain reflections arising from the compound under study. No other reflections were observed in the patterns.

Magnetic Measurements. Magnetic susceptibility measurements were performed with a Quantum Design Model MPMS XL 5T SQUID susceptometer in the temperature range of 1.8−300 K, using powder samples (30 mg) loaded into gelatin capsules. Variable temperature data were collected under an applied magnetic field of 100 Oe and corrected for the diamagnetic contribution of the gelatin capsules. Magnetization (M vs H) data were collected at 2 K and for $-5\ \text{T} \leq H \leq 5\ \text{T}$.

Surface Area Determination. The surface area of the nitrides were determined where appropriate by applying the Brunauer−Emmett−Teller (BET) method to nitrogen physisorption isotherms determined at liquid nitrogen temperatures. Isotherms were measured using a Micromeritics Model Flow Prep 060 Gemini BET machine. The samples were degassed at 383 K overnight to remove any adsorbed moisture prior to analysis.

Elemental Analysis. Carbon, hydrogen, and nitrogen (CHN) analysis of the content of samples was determined by combustion, using an Exeter Analytical Model CE-440 elemental analyzer.

Results and Discussion

Synthesis and Reactivity of Co_3Mo_3N. We have observed that the form of cobalt molybdate starting material is of vital importance to the successful synthesis of Co_3Mo_3N. Pure-phase 331 nitride is only found when using *hydrated* cobalt molybdate ($CoMoO_4 \cdot nH_2O$) as a precursor in the ammonolysis reaction; dehydrated polymorphs of $CoMoO_4$ produce multiphase products, following treatment with NH_3. Furthermore, following ammonolysis and passivation, pretreatment in 3:1 H_2/N_2 for 2 h at 973 K is essential to obtain well-crystallized Co_3Mo_3N powders. The PXD patterns of the material prepared in this manner and those of the products at intermediate steps of the synthesis process are shown in Figure 2. The first intermediate product following treatment of the $CoMoO_4 \cdot nH_2O$ precursor could be tentatively identified as a dehydrated cobalt molybdate (by comparison to patterns of $MnMoO_4$),[27] whereas the initial ammonolysis product was very poorly crystalline by PXD and could not be identified. The final product can be matched exclusively to the Co_3Mo_3N phase. The nitrogen content of this material, which has a BET surface area of 18 m^2/g, has been determined by combustion analysis to be 2.8(3) wt %, which compares well to the expected value of 2.93 wt %. The ammonia synthesis activity of this material at 400 °C has been measured as 167 μmol g^{-1} h^{-1}, which is in reasonable agreement with other studies in the literature.[11] Post-reaction analysis shows that no changes in phase composition occur upon reaction (i.e., the reaction product is also single-phase). At higher temperatures, we have demonstrated the reactivity of the lattice nitrogen species in Co_3Mo_3N through its removal in temperature-programmed reactions using 3:1 H_2/Ar. Accordingly, we have shown that it is possible to remove 50% of the lattice nitrogen at a reaction temperature of 973 K, with the post-reaction nitrogen content being measured as 1.5(3) wt % by CHN analysis (hence implying a Co:Mo:N ratio of 6:6:1). Hydrogen is necessary for this loss to occur, demonstrating that the process is not simply thermal decomposition. In addition, nitrogen is not further depleted (beyond 50% removal) at longer reaction times. The 50% loss of nitrogen is

(27) Abrahams, S. C.; Reddy, J. M. *J. Chem. Phys.* **1995**, *43*, 2533.

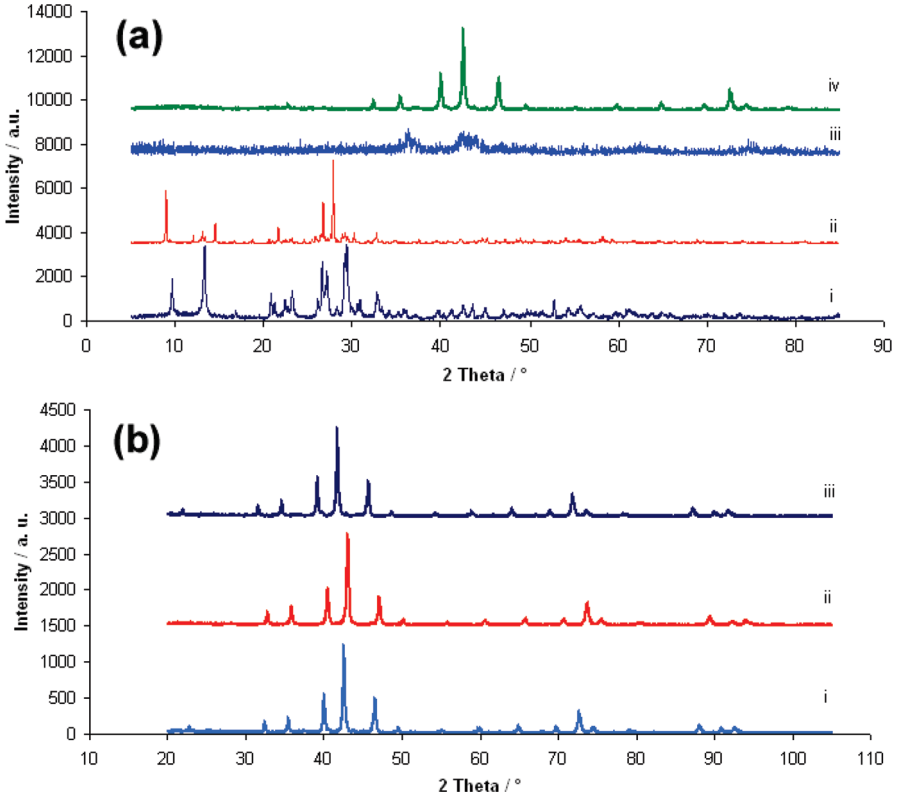

Figure 2. XRD patterns of Co−Mo materials at each stage of processing, showing (a) the formation of Co_3Mo_3N ((i) $CoMoO_4 \cdot nH_2O$, as prepared by precipitation; (ii) Co−Mo−O precursor, following calcination at 773 K for 3 h in air; (iii) product following ammonolysis of the cobalt molybdate precursor under the heating regime in Figure 1a, and (iv) Co_3Mo_3N phase formed following subsequent passivation and prereaction treatment under flowing 3:1 H_2/N_2 at 973 K) and (b) the formation of Co_6Mo_6N and regeneration to Co_3Mo_3N ((i) Co_3Mo_3N formed as above, (ii) Co_6Mo_6N phase formed following denitridation of Co_3Mo_3N under H_2/Ar following the heating regime in Figure 1b, and (iii) Co_3Mo_3N produced after renitridation under 3:1 H_2/N_2 at 973 K, for 4 h).

accompanied by a change in the cubic lattice parameter (a) from 11.020(1) Å (331 phase) to 10.881(1) Å (661 phase). Crucially, in terms of potential application, it is possible to restore the 661 phase to the original 331 phase by heating under 3:1 H_2/N_2 (see Figure 2b). The nitrogen content increases again to 2.8(3) wt % and the value of parameter a of the restored material is 11.025(4) Å, which is in excellent agreement with that for the prereacted 331 phase. Therefore, the PXD and combustion analysis data might indicate that there is a single transformation from a 331 phase to a 661 phase on reduction, as opposed to the formation of a continuum of stoichiometries and structures. To confirm this suggestion and to explore the premise that the 661 phase was a nitride analogue to the η-12 carbide, Co_6Mo_6C, it was necessary to not only refine possible structural models against PXD data but also to determine the structure of the 661 phase using PND data, such that the quantity and location of lattice nitrogen could be established unequivocally. The results of these studies, along with those of the magnetic properties of the 331 and 661 phases, are given below.

Structure of the 331 Phase: Co_3Mo_3N. The structure derived from the Rietveld refinement against PXD data conforms closely to the η-6 carbide model proposed for Fe_3Mo_3N and Co_3Mo_3N structures by zur Loye et al. (see Table 1). The nitride thus crystallizes in cubic space group $Fd\bar{3}m$ (cell setting 2 is used herein), forming a filled Ti_2Ni structure, as previously reported in the literature and isotypic with the equivalent carbide, Co_3Mo_3C. The PXD refinement reached a minimum with the nonmetal 16c site fully occupied by the nitrogen and the 8a site vacant (see Figure S1 in the Supporting Information). When the nitrogen stoichiometry was refined freely, the occupation of the 16c site converged at unity, in agreement with the nitrogen content obtained from the CHN analysis of the samples (2.8(3) wt %) and consistent with a formula of Co_3Mo_3N for the nitride.

Table 1. Crystallographic Parameters for Co_3Mo_3N, for Various Diffraction Methods and Data Collection Temperatures

parameter	Value		
	X-ray, 298 K	ToF neutron, 290 K	ToF neutron, 4.2 K
compound		Co_3Mo_3N	
color of powder	black	black	black
formula mass (g/mol)	478.62	478.62	478.62
crystal information			
crystal system	cubic	cubic	cubic
space group	$Fd\bar{3}m$	$Fd\bar{3}m$	$Fd\bar{3}m$
Z	16	16	16
cell parameter, a (Å)	11.0203(5)	11.0146(1)	10.9808(2)
unit-cell volume, V (Å^3)	1338.38(10)	1336.30(3)	1324.05(4)
calculated density, ρ_x (g/cm^3)	9.501	9.516	9.604
number of observations	4959	11683	11635
number of variables	26	60	63
R_p (%)	14.84	2.76	1.59
R_{wp} (%)	20.31	1.94	1.07
χ^2	1.41	3.27	2.64

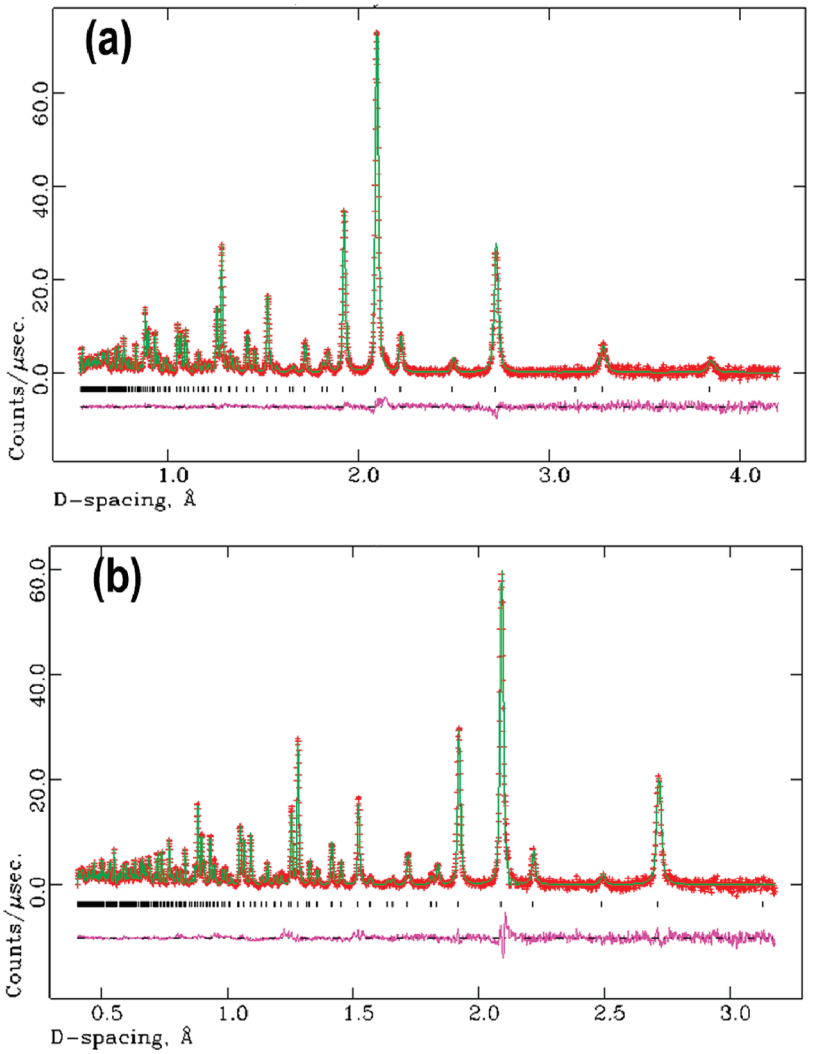

Figure 3. Observed, calculated, and difference profile plots for the Rietveld refinement against powder neutron diffraction data for Co_3Mo_3N at (a) 290 K and (b) 4.2 K. Crosses show the observed data points, solid lines represent the calculated diffraction patterns, and tick marks represent the calculated positions of the reflections. The data shown are from detectors positioned at $\langle 2\theta \rangle = 90°$ and $\langle 2\theta \rangle = 145°$, respectively.

To confirm that the findings of the XRD refinements were accurate, PND experiments were performed on the samples. The refined models from the XRD refinements were used as starting models for the PND refinements. Room-temperature neutron data were used to validate the structure proposed by XRD; in addition, given the magnetic data obtained (see below), diffraction data were collected at low temperature to identify any possible magnetic ordering that was present in the samples that would be manifest as enhanced peak intensities or additional magnetic reflections.

Results from room-temperature PND refinements (see Figure 3a) showed very strong agreement to the proposed structure of Co_3Mo_3N from XRD data. The cubic $Fd\bar{3}m$ η-6 carbide structural model from completed refinement against room-temperature data was used successfully as the starting model for the low-temperature measurement. The low-temperature PND experiment (Figure 3b) showed no signs of magnetic scattering (increased intensities or new Bragg reflections), and hence that there is no neutron diffraction evidence for magnetic ordering. PND data at both temperatures, therefore, support a model in which nitrogen exclusively and fully occupies the *16c* (0,0,0) site. Alternative models in which nitrogen was placed on the 8a site converged with higher residuals and poorer profile fits to the previously established η-6 carbide model. Final crystallographic data and refined atomic parameters from each of the diffraction experiments are shown in Tables 1 and 2, respectively. Selected interatomic distances and angles are displayed in Table 3. The structure of Co_3Mo_3N, particularly highlighting the Mo and N sublattices, is shown in Figure 4, while the coordination environments for Co(1), Co(2), Mo, and N are depicted in more detail in Figure 5. The η-6 carbide structure, as derived from filling the Ti_2Ni structure, is discussed fully elsewhere,[7,21,25,28] and we focus briefly here on the local environment around the individual constituent atoms. The metal atoms (here, Co and Mo) occupy three special positions—with site symmetry of 32e, 16d, and 48f, respectively. In the η-6 carbide, the interstitial 16c (0, 0, 0) site is occupied (in this case, by N).

(28) Nyman, H.; Andersson, S.; Hyde, B. G.; O'Keeffe, M. *J. Solid State Chem.* **1978**, *26*, 123.

Table 2. Refined Atomic Parameters for Co_3Mo_3N for Different Diffraction Data and Data Collection Temperatures

parameter	Value: X-ray, 293 K	Value: ToF neutron, 290 K	Value: ToF neutron, 4.2 K
Co(1), 32e (x, x, x)			
x	0.2919(2)	0.29214(5)	0.29221(7)
occupancy	1	1	1
$U_{11} = U_{22} = U_{33}$ ($\times 10^{-2}$ Å^2)	1.11(13)	0.468(17)	0.22(2)
$U_{12} = U_{13} = U_{23}$ ($\times 10^{-2}$ Å^2)	0.06(13)	−0.053(17)	−0.07(2)
Co(2), 16d ($^1/_2$, $^1/_2$, $^1/_2$)			
occupancy	1	1	1
$U_{11} = U_{22} = U_{33}$ ($\times 10^{-2}$ Å^2)	0.56(19)	0.40(2)	0.08(2)
$U_{12} = U_{13} = U_{23}$ ($\times 10^{-2}$ Å^2)	−0.29(21)	−0.13(3)	−0.07(3)
Mo, 48f (x, $^1/_8$, $^1/_8$)			
x	0.3242(2)	0.32398(3)	0.32462(4)
occupancy	1	1	1
U_{11} ($\times 10^{-2}$ Å^2)	0.85(15)	0.562(12)	0.112(15)
$U_{22} = U_{33}$ ($\times 10^{-2}$ Å^2)	0.94(10)	0.341(7)	0.134(9)
U_{23} ($\times 10^{-2}$ Å^2)	0.19(14)	−0.125(9)	−0.107(12)
N, 16c (0, 0, 0)			
occupancy	1	1	1
$U_{11} = U_{22} = U_{33}$	0.75	0.493(8)	0.297(9)
$U_{12} = U_{13} = U_{33}$	0	0.030(8)	0.007(10)

Table 3. Selected Interatomic Distances and Angles for Co_3Mo_3N from ToF Neutron Diffraction Data at Various Data Collection Temperatures

	Value: 290 K	Value: 4.2 K
Atomic Distance (Å)		
N−Mo × 6	2.1109(1)	2.1072(2)
Mo−Mo × 3	2.8659(1)	2.8543(2)
Mo−Mo × 3	3.1001(4)	3.1007(5)
Co(1)−Mo × 3	2.6275(7)	2.6216(9)
Co(1)−Mo × 3	2.7274(3)	2.7129(4)
Co(1)−Co(1) × 3	2.5805(16)	2.570(2)
Co(1)−Co(2) × 3	2.3816(3)	2.3737(4)
Co(2)−Mo × 6	2.7475(2)	2.7340(3)
Co(2)−Co(1) × 6	2.3816(3)	2.3737(4)
Bond Angle (°)		
N−Mo−N	134.56(2)	134.20(2)
Mo−N−Mo × 6	94.50(1)	94.74(1)
Mo−N−Mo × 6	85.50(1)	85.26(1)
Mo−N−Mo × 3	180.0	180.0

The occupation of the 16c site confers a slightly distorted octahedral coordination geometry on the nonmetal, which is coordinated exclusively to the metal in the 48f site (Mo). Hence, by filling the interstitial site, the immediate environment of the metals (Co) on the 32e and 16d sites is unchanged, relative to the hypothetical alloy ("CoMo"), whereas the coordination number of the 48f site (Mo) increases by 2 (see Figure 5c). The Co sublattice (composed of Co supertetrahedra; Co in the 32e positions forming tetrahedra capped on each face by Co in 16d sites) is thus regarded as a metallic network, whereas the Mo−N vertex sharing octahedra can be regarded as relatively ionic. The nature of these component parts of the structure is reflected in the interatomic distances. The Co−Co distances compare favorably to those in α-Co

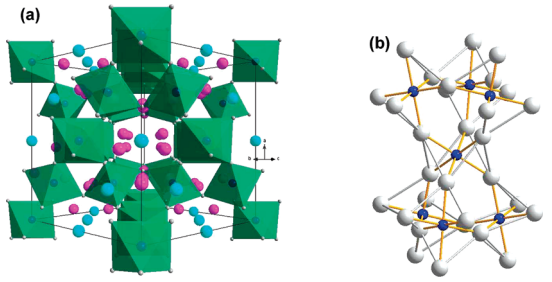

Figure 4. Structure of Co_3Mo_3N: (a) polyhedral plot illustrating the NMo_6 octahedra (green polyhedra) and the location of the Co atoms on the 32e (Co(1) is represented by magenta spheres) and 16d sites (Co(2) is represented by light blue spheres); (b) detail of the Mo−N sublattice, illustrating the filling of the 16c site by nitrogen. Gray and dark blue spheres represent Mo and N atoms, respectively.

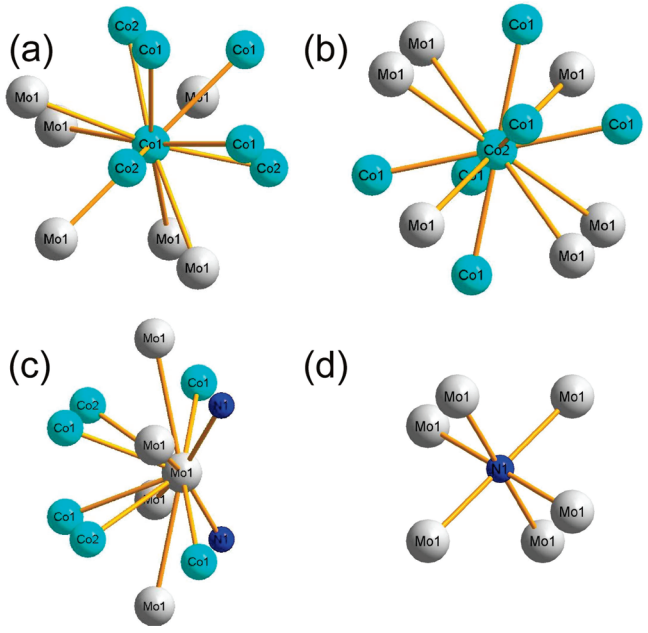

Figure 5. Coordination geometry at (a) the Co(1) (32e) site, (b) the Co(2) (16d) site, (c) the Mo (48f) site, and (d) the N (16c) site in Co_3Mo_3N. Light blue, gray, and dark blue spheres represent Co, Mo, and N, respectively.

metal (2.51 Å)[29] whereas the Mo−N distances closely resemble those in Fe_3Mo_3N[30] and, for example, $LiMoN_2$ (2.095(4) Å).[31]

Structure of the 661 Phase; Co_6Mo_6N. Rietveld refinement against PXD data produced several possible solutions to the structure of the cubic Co_6Mo_6N phase in which the cell parameter is reduced *cf*, Co_3Mo_3N. Marginally, the best fit was obtained for a structure isotypic to the η-12 carbide Co_6Mo_6C (also cubic $Fd\bar{3}m$) in which the nitrogen occupies the 8a site in the Ti_2Ni-derived structure and the 16c is vacant (populating the 16c site with nitrogen to half-occupancy increased the value of R_{wp} by 0.6% and χ^2 by 0.1) (see Figure S2 in the Supporting Information). When the nitrogen stoichiometry was refined freely, the occupation of the 8a site converged at unity, in agreement with the nitrogen content obtained

(29) Taylor, A.; Floyd, R. *Acta Crystallogr.* **1950**, *3*, 285.
(30) Bem, D. S.; Gibson, C. P.; zur Loye, H.-C. *Chem. Mater.* **1993**, *5*, 397.
(31) Elder, S. H.; Doerrer, L. H.; DiSalvo, F. J.; Parise, J. B.; Guyomard, D.; Tarascon, J. M. *Chem. Mater.* **2002**, *4*, 928.

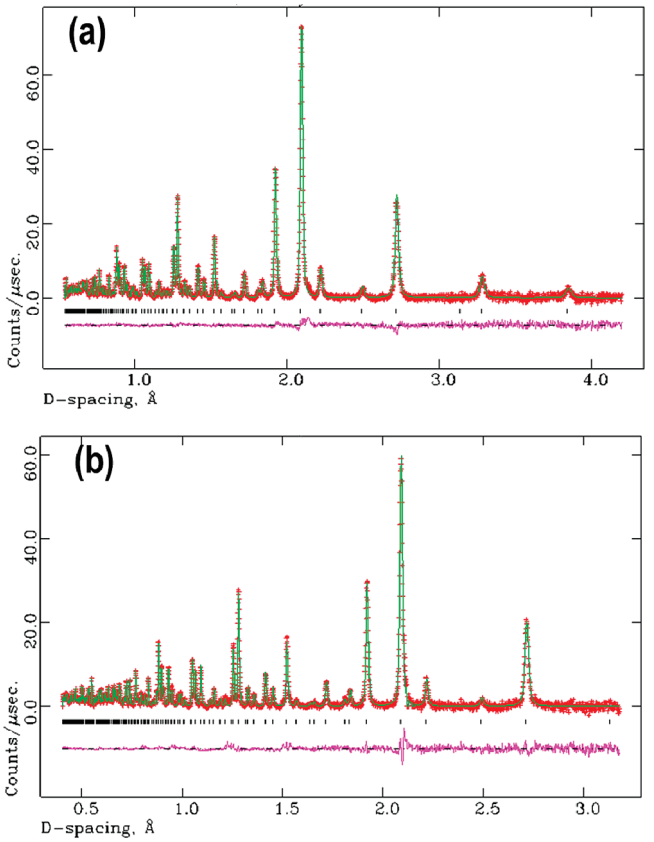

Figure 6. Observed, calculated, and difference profile plot for the Rietveld refinement against powder neutron diffraction data for Co_6Mo_6N at (a) 290 K and (b) 4.2 K. Crosses show the observed data points, solid lines represent the calculated diffraction patterns, and tick marks represent the calculated positions of the reflections. The data shown are from detectors positioned at $\langle 2\theta \rangle = 90°$ and $\langle 2\theta \rangle = 145°$, respectively.

from the CHN analysis of the samples (1.5(3) wt %) and consistent with a formula of Co_6Mo_6N for the nitride.

The η-12 carbide model from the XRD refinement above was used as a starting model for the PND refinements. Room-temperature neutron data were used to test the η-12 carbide structure proposed by XRD, and, once again, given the results of magnetic measurements (see below), diffraction data were collected at low temperature to identify any possible long-range magnetic ordering in the 661 sample that might be visible as magnetic contributions to the scattering.

Data from the room-temperature PND refinement (Figure 6a) supported the proposed η-12 carbide structure as the most likely candidate for Co_6Mo_6N and a similar strong preference was obtained using the η-12 model as the basis for the low-temperature refinement. Similar to our experience with the 331 nitride, the low-temperature PND experiment (see Figure 6b) showed no evidence of increased intensities or new Bragg reflections, and, on this basis, the possibility of long-range magnetic ordering could be discarded. However, given the relatively small differences in the values of the *R*-factors and the goodness-of-fits for various applied models in the XRD refinements of the 661 samples above, it was important that we tested fully the possible site distribution models for nitrogen in the reduced nitride phase. By contrast to the PXD refinements and, as might be expected, by the vastly different relative scattering power of nitrogen, compared to the other constituent elements under neutrons, the alternative models that we investigated produced results that were readily distinguishable in terms of the quality of fits, the physical meaning of the figures obtained, and the errors associated with the refined parameters. Furthermore, the contrast in the difference profiles of the refinement plots presented an immediate and vivid indication of the relative value of the alternative models. Hence, the PND data, both at 4.2 and 290 K, support unequivocally a model in which nitrogen fully occupies the 8a ($^1/_8$,$^1/_8$,$^1/_8$) site only. The presence of nitrogen on the 8a site (and, conversely, its absence on the 16c site) was verified further by reference to difference Fourier maps of the nuclear density (see the Supporting Information). Final crystallographic data and refined atomic parameters from each of the diffraction experiments are shown in Tables 4 and 5, respectively. Selected interatomic distances and angles are displayed in Table 6.

Table 4. Crystallographic Parameters for Co_6Mo_6N

parameter	Value: X-ray, 298 K	ToF neutron, 290 K	ToF neutron, 4.2 K
color of powder	black	black	black
formula mass (g/mol)	943.25	943.25	943.25
crystal information			
crystal system	cubic	cubic	cubic
space group	$Fd\bar{3}m$	$Fd\bar{3}m$	$Fd\bar{3}m$
Z	8	8	8
cell parameter, a (Å)	10.8824(16)	10.87970(9)	10.85596(15)
unit-cell volume, V (Å^3)	1288.8(3)	1287.81(2)	1279.39(3)
calculated density, ρ_x (g/cm^3)	9.723	9.730	9.794
number of observations	5076	12325	12063
number of variables	25	58	57
R_p (%)	13.41	2.50	1.42
R_{wp} (%)	19.27	1.28	0.85
χ^2	1.21	1.09	1.60

Table 5. Refined Atomic Parameters for Co_6Mo_6N

parameter	Value: X-ray, 293 K	ToF neutron, 290 K	ToF neutron, 4.2 K
Co(1), 32e (x, x, x)			
x	0.2919(2)	0.29226(3)	0.29215(6)
occupancy	1.0	1.0	1.0
$U_{11} = U_{22} = U_{33}$ ($\times 10^{-2}$ Å^2)	1.12(12)	0.451(10)	0.15(2)
$U_{12} = U_{13} = U_{23}$ ($\times 10^{-2}$ Å^2)	0.08(13)	−0.077(11)	−0.15(2)
Co(2), 16d ($^1/_2$, $^1/_2$, $^1/_2$)			
occupancy	1.0	1.0	1.0
$U_{11} = U_{22} = U_{33}$ ($\times 10^{-2}$ Å^2)	1.25(19)	0.409(12)	0.11(2)
$U_{12} = U_{13} = U_{23}$ ($\times 10^{-2}$ Å^2)	0.09(18)	0.054(15)	0.11(3)
Mo, 48f (x, $^1/_8$, $^1/_8$)			
x	0.32094(18)	0.32126(2)	0.32176(3)
occupancy	1.0	1.0	1.0
U_{11} ($\times 10^{-2}$ Å^2)	0.77(14)	0.349(8)	0.087(13)
$U_{22} = U_{33}$ ($\times 10^{-2}$ Å^2)	0.92(9)	0.395(5)	0.098(8)
U_{23} ($\times 10^{-2}$ Å^2)	−0.08(13)	0.045(7)	0.007(13)
N, 8a ($^1/_8$, $^1/_8$, $^1/_8$)			
occupancy	1.0	1.0	1.0
$U_{11} = U_{22} = U_{33}$ ($\times 10^{-2}$ Å^2)	1.00	0.492(6)	0.399(12)

Table 6. Selected Interatomic Distances and Angles for Co_6Mo_6N at Various Data Collection Temperatures

parameter	Value	
	290 K	4.2 K
	Atomic Distances (Å)	
N−Mo × 6	2.1353(2)	2.1361(4)
Mo−Mo × 3	2.8428(1)	2.8344(2)
Mo−Mo × 3	3.0198(3)	3.0210(5)
Co(1)−Mo × 3	2.5927(5)	2.5863(8)
Co(1)−Mo × 3	2.7206(2)	2.7095(3)
Co(1)−Co(1) × 3	2.5462(10)	2.5439(18)
Co(1)−Co(2) × 3	2.3518(2)	2.3474(4)
Co(2)−Mo × 6	2.7350(1)	2.7252(3)
Co(2)−Co(1) × 6	2.3518(2)	2.3474(4)
	Bond Angles (°)	
N−Mo−N	162.716(5)	162.877(10)
Mo−N−Mo × 6	90.0	90.0
Mo−N−Mo × 6	90.0	90.0
Mo−N−Mo × 3	180.0	180.0

The individual coordination environments for Co(1), Co(2), Mo, and N are depicted in Figure 7.

The consequences of the non-metal (N) occupying the 8a site, as opposed to the 16c site, are several-fold. First, although the Co(−Co) sublattice is essentially unchanged in structure, the intermetallic distances decrease, resulting in an overall contraction of the sublattice in the 661 phase. This could have implications for magnetic and electronic properties for η-carbides and is discussed more fully in the following section. Second, the unique Mo−N distance increases by ca. 1% and, hence, the Mo−N sublattice expands in the η-12 nitride; the distortion of the Mo−N octahedron in the η-6 nitride is removed. Finally, both the Co−Mo and Mo−Mo distances decrease and, hence, although the Co(1)−Co(2) and Mo−N sublattices might still be regarded as "independent", the interaction between them could be perceived as increasing as nitrogen is removed from the structure. It is pertinent to consider briefly the crystal chemistry implications of the preferential 8a site filling in the reduced nitride. The Mo−N

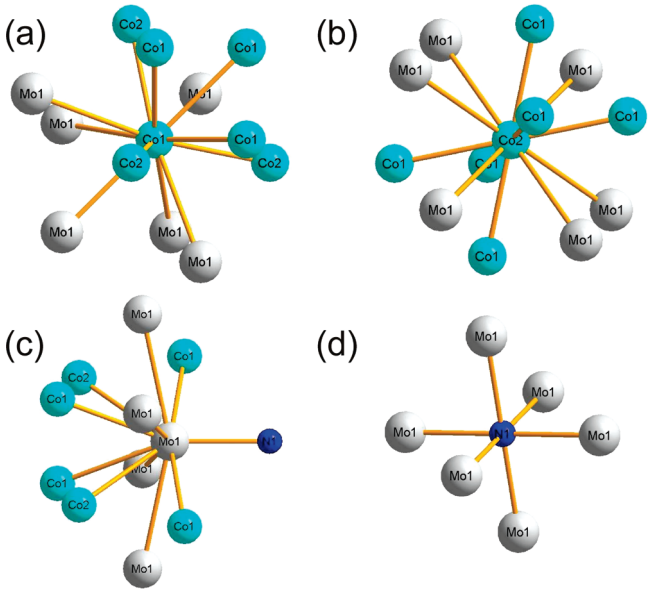

Figure 7. Coordination geometry at (a) the Co(1) (32e) site, (b) the Co(2) (16d) site, (c) the Mo (48f) site, and (d) the N (8a) site in Co_6Mo_6N. Light blue, gray, and dark blue spheres represent Co, Mo, and N, respectively.

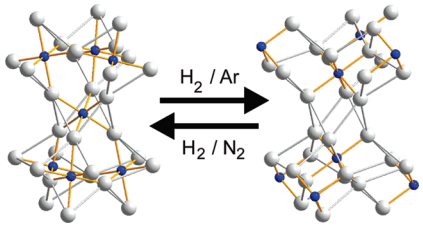

Figure 8. Mo−N sublattices in Co_3Mo_3N (left) and Co_6Mo_6N illustrating the migration of nitrogen from the 16d site in Co_3Mo_3N to the 8a site in Co_6Mo_6N. Gray and dark blue spheres represent Mo and N, respectively.

distance increases from 2.111 Å to 2.135 Å from the 331 phase to the 661 phase, as a result of the N migration from the 16c site to the 8a site. Were the 16c position to remain the site of choice—at half occupation—on denitrogenation, the equivalent Mo−N bond lengths would be constrained at a relatively short distance of ca. 2.07 Å by the symmetry of the N position (a distance still appreciably longer than those found in nominally ionic ternary molybdenum(VI) nitrides, such as $Ca(Ba)_3MoN_4$).[32]

In their study of the structure of M_3Mo_3N (where M = Fe, Co) by a combined refinement against PXD and PND data, Jackson et al. commented on how the nitrides contravene the empirical observation made by Mackay et al.[33] in η-carbide structured suboxides that the non-metal site preference (16c vs 8a) correlates to the position of the metal (Mo in Co_3Mo_3N) located in the 48f site (x, $^1/_8$, $^1/_8$). For these η-carbide structure oxides, when $x > 0.3125$ (with $x = 0.3125$ being the ideal Ti(2) position in Ti_2Ni), the 8a site is preferentially filled by the non-metal (O). In fact, the equivalent carbides had already been shown to contravene this relationship and, subsequently, all the intermediate 331 compounds studied in the $Fe_{3-x}Co_xMo_3N$ solid solution were observed with the same N site preference (and values of x(Mo) > 0.3125) as the end members (i.e., with $x = 0$ and $x = 3$). The same is true for our room-temperature structure solution for Co_3Mo_3N (with x(Mo) ≈ 0.324) and one can conclude, therefore, and perhaps unsurprisingly, that the bonding and minimum energy structures in the 331 phase nitrides are more similar to the equivalent carbides than to oxides with η-carbide structures. A recent atomistic simulation study would seem to reinforce this contrast where, for both Fe_3Mo_3N and Co_3Mo_3N, N was shown to occupy the 16c site in the energy-minimized structures and coincide with x(Mo) ≈ 0.33.[34] In fact, the x coordinate of the Mo position does not change markedly from the 331 phase to the 661 phase ($x \approx 0.321$ in the latter; the 8a site now is filled exclusively) and, hence, one is again bound to conclude that a limiting Mo position of $x >$ 0.3125 is not a defining parameter in the determination of interstitial site filling in the η-carbide nitrides. (See Figure 8.)

(32) Baker, C. F.; Barker, M. G.; Blake, A. J.; Wilson, C.; Gregory, D. H. *Dalton Trans.* **2003**, 1065.
(33) Mackay, R.; Miller, G. J.; Franzen, H. F. *J. Alloys Compd.* **1994**, *204*, 109.
(34) Chen, Y.; Shen, J.; Chen, N.-X. *Solid State Commun.* **2009**, *149*, 121.

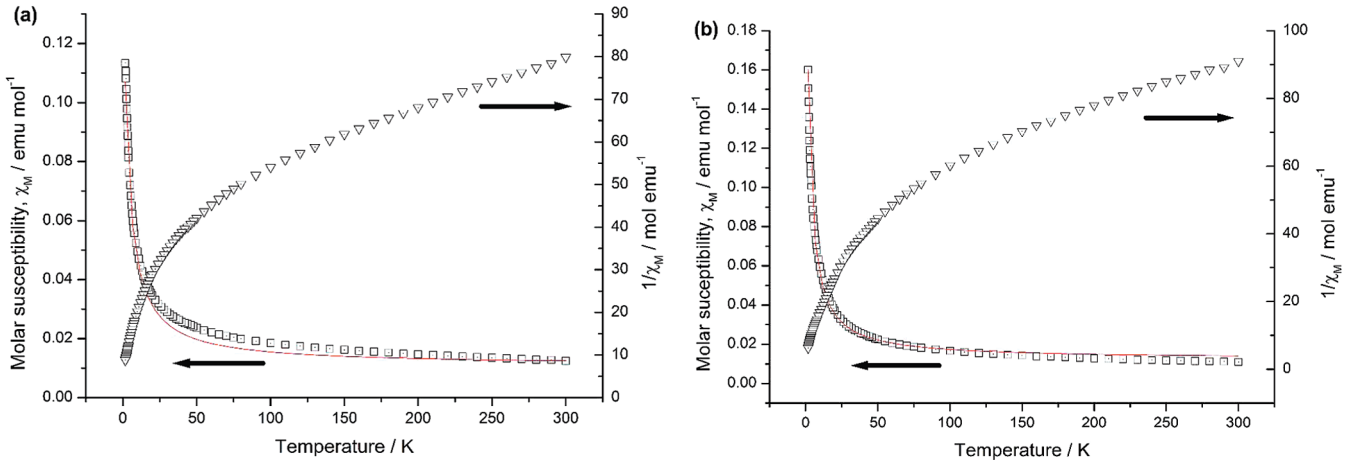

Figure 9. Plot of (□) the molar magnetic susceptibility and (△) the inverse of the mass magnetic susceptibility against temperature (T) for (a) Co_3Mo_3N and (b) Co_6Mo_6N. The red solid curves represent the best (P + C−W) fits to the χ_M vs T data.

Magnetic Behavior of the 331 and 661 Phases. The mass susceptibility was measured as a function of temperature for Co_3Mo_3N and Co_6Mo_6N at 5000 Oe, yielding the plots shown in Figure 9. The susceptibility (and inverse susceptibility) is linear, with only a gentle gradient for *ca.* 100 K $\leq T \leq$ 300 K in both compounds with a large increase in gradient below this temperature range. The profile of the susceptibility closely resembles that observed by zur Loye et al., suggesting that the susceptibility is non-Curie-like and our χ_M vs T data can be fit to a modified Curie−Weiss (C−W) expression, incorporating a temperature-independent term to represent the Pauli (P) paramagnetic component to the magnetism. Conversely, attempts to fit the perceived linear portion of the $1/\chi_M$ vs T plots (i.e., from the C−W-only expression) were not successful. The P + C−W fits yield tentative values for C, θ, and χ_0 of 0.468(6) emu mol^{-1} K, 3.186(7) K, 0.011(1) emu mol^{-1} and 0.499(1) emu mol^{-1} K, 1.688(6) K, and 0.012(1) emu mol^{-1} for the 331 and 661 phases, respectively. The values of θ would indicate a tendency to weak local ferromagnetic interactions, which diminish from the 331 phase to the 661 phase.

There are no obvious magnetic transitions present in the variable temperature data as our PND results would also suggest. Prior and Battle demonstrated that, in the $Fe_{3-x}Co_xMo_3N$ solid solution, there seems to be no obvious systematic variation in magnetic behavior with composition or, therefore, with valence electron counting principles.[7] Fe_2CoMo_3N, for example, was revealed to be superparamagnetic whereas $FeCo_2Mo_3N$ is essentially Pauli paramagnetic. In a more recent study, it was demonstrated that long-range magnetic ordering could be tuned by partially substituting nonmagnetic elements onto the 16d site and that the strength of these interactions was correlated to the distance between magnetic atoms (Co, Fe) on the 32e sites.[35] Although reasonable fits were obtained for a C−W + P model to our magnetic data in each case above, given the steep slope of the "Curie tails" at low temperature (with approximate onset temperatures of 90 and 100 K for the 331 and 661 phases, respectively, at the point of the sharp change in gradient) and the precedent for deviation from paramagnetic behavior in nitrides with the η-6 carbide structure, we examined the magnetization behavior as a function of field at 2 K for both the 331 and 661 nitride. The results of the M vs H measurements are shown in Figure 10.

The magnetization plots show that neither the 331 phase nor the 661 phase exhibit a linear profile with applied field. Furthermore, both compounds exhibit only a weak and almost negligible hysteresis manifested in a nominal coercive field ($H_c \approx$ 20 Oe and 4 Oe for the 331 and 661 nitrides, respectively). Equally, however, the magnetization of neither sample saturates, even under a maximum applied field of 5 T. The differences in the magnetism between the 331 and 661 phases are subtle but reproducible, suggesting that the magnetism is intrinsic to the materials and probably a function of the crystal chemistry rather than the microstructure of the samples, although we cannot completely rule out the possibility of very low levels of ferromagnetic impurity (below the diffraction detection limits). The small positive Weiss constants from the fits to the temperature dependence of the susceptibility and the weak hysteresis in the M vs H measurements suggest localized ferromagnetic interactions within the $Co(1)_4$ tetrahedra in both the 331 and 661 phases. The reduction in the Co(1)−Co(1) distances upon the removal of nitrogen (331 to 661 phases) would insinuate increased ferromagnetism. If one assumes similar magnetic structural models for the Co η-carbides to those for the magnetically ordered substituted phases described recently,[35] then one would expect each $Co(1)_4$ tetrahedron to couple antiferromagnetically to its nearest neighbors through the face capping Co(2) atoms on the 16d sites. We are in the process of investigating these relationships and possible correlations between magnetism and microstructure further.

Furthermore, in ongoing studies employing isotopically labeled nitrogen, we are investigating the nitrogen activation and desorption properties of the Co_3Mo_3N and the Co_6Mo_6N phases. The comparison between

(35) Sviridov, L. A.; Battle, P. D.; Grandjean, F.; Long, G. J.; Prior, T. J. *Inorg. Chem.* **2010**, *49*, 1133.

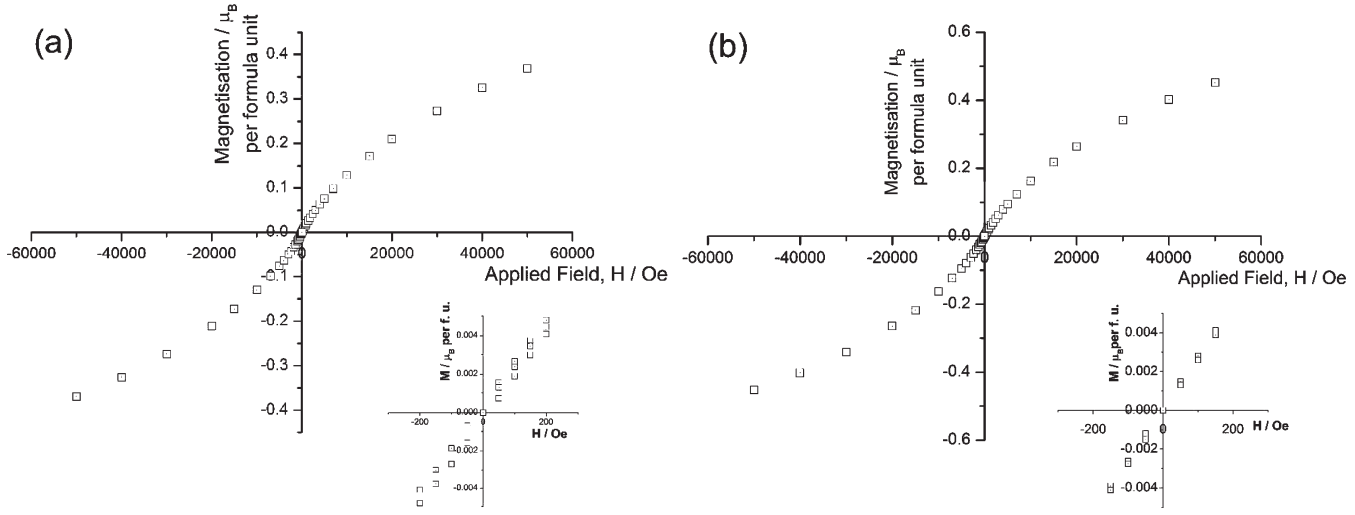

Figure 10. Magnetization of (a) Co_3Mo_3N and (b) Co_6Mo_6N as a function of applied field at 2 K. The inset illustrates the detail of the *M* vs *H* behavior around the origin.

homomolecular exchange kinetics (in which $^{14}N_{2(g)}$ and $^{15}N_{2(g)}$ are scrambled), and heterolytic exchange kinetics (in which an exchange between $^{15}N_{2(g)}$ and lattice N occurs) will be used to yield information on the relative reactivity of adsorbed nitrogen versus lattice nitrogen. Additional studies are also being targeted toward the microstructural effects upon catalytic activity, as well as the transformation process.[36]

Conclusion

We have demonstrated that treatment of cobalt molybdenum nitride (Co_3Mo_3N) with the η-6 carbide structure, under a hydrogen−argon mixture, results in the loss of 50% of the lattice nitrogen and formation of the new nitride, Co_6Mo_6N. This 661 phase forms with the η-12 carbide structure. The 331 phase can be regenerated by heating under hydrogen−nitrogen and cycling between the η-6 and η-12 nitrides is topotactic and fully reversible; nitrogen migrates between the 16c and 8a sites. One can thus view the 331 nitride as a reservoir of activated nitrogen that can be released and replenished and could be utilized as a nitrogen storage medium. The denitrided 661 phase shows no long-range magnetic order, which is similar to that observed for the fully nitrided parent.

Acknowledgment. The authors thank Dr. R. W. Hughes for his assistance with the neutron data collection. We also thank Mrs. K. Wilson for kindly performing CHN analysis. D.H.G. and J.S.J.H. thank the EPSRC for a DTA studentship for S.M.H.. J.S.J.H. also thanks the EPSRC for financial support (under Grant No. GR/S873001).

Supporting Information Available: Nuclear density maps for room-temperature refinements of Co_3Mo_3N and Co_6Mo_6N. This information is available free of charge via the Internet at http://pubs.acs.org/.

(36) See, for example: Alconchel, S.; Sapina, F.; Beltran, D.; Beltran, A. *J. Mater. Chem.* **1999**, *9*, 749.